On the radiation force fields of fractional order acoustic vortices

Z. Y. Hong,[1,2(a)] J. Zhang[2] and B. W. Drinkwater[2(b)]

[1]Department of Applied Physics, Northwestern Polytechnical University, Xi'an 710072, China

[2]Department of Mechanical Engineering, University Walk, University of Bristol, Bristol BS8 1TR, UK

Abstract - Here we report the creation and observation of acoustic vortices of fractional order. Whilst integer orders are known to produce axisymmetric acoustic fields, fractional orders are shown to break this symmetry and produce vast array of unexplored field patterns, typically exhibiting multiple closely-spaced phase singularities. Here, fractional acoustic vortices are created by emitting ultrasonic waves from an annular array of sources using multiple ramps of phase-delay around its circumference. Acoustic radiation force patterns, including multiple concentration points, short straight lines, triangles, squares and discontinuous circles are simulated and experimentally observed. The fractional acoustic vortex leading to two closely spaced phase singularities is used to trap, and by controlling the order, reversibly manipulate two microparticles to a proximity of 0.3 acoustic wavelengths.

PACS 43.25.Qp - Radiation pressure

PACS 43.35.Ty - Other physical effects of sound

Key words: acoustic vortices, fractional topological charge, trap patterns, wavelength-scale

(a) E-mail: hongzy@nwpu.edu.cn

(b) E-mail: B.Drinkwater@bristol.ac.uk

Introduction. - Since 1974, waves with helicoidal wavefronts have attracted increasing interest in the fields of acoustics [1], optics [2] and quantum mechanics [3]. These waves are usually called vortices, characterized by an azimuthal, θ phase dependence of the form $e^{-im\theta}$, where the integer m is the order or topological charge of the helicoidal beam and this encodes the angular rotation rate of the wavefront. These vortices possess orbital angular momentum, a central zero/low intensity phase singular point and have found application in trapping and rotating of microparticles [4-9] as well as in communications [10,11].

Recently, vortices with fractional (*i.e.* non-integer) orders have been explored in the optical field [12-21]. The axis-symmetry of intensity found in integer-order optical vortices is broken for non-integer orders and a low-intensity radial strip has been observed. This low-intensity strip has been proposed as a channel for radially transferring particles into and out of the vortex core [13]. Additionally, fine adjustment of the order of optical vortices has been suggested as a means of controlling the orbital angular momentum [17]. Compared with optical vortices, acoustic vortices can provide larger torques [7-9] and higher trapping forces [22-24] to various matter with no limitation on their electromagnetic properties. However, despite the potential advantages of acoustics in some applications, the acoustic counterparts of various optical phenomena, such as fractional vortices and knots [25] have yet to be explored.

In this paper, we employ an annular array consisting of 64 ultrasonic sources to create two-dimensional fractional acoustic vortices and experimentally observe their ability to pattern microparticles. Modeling using finite element analysis is also used to simulate the acoustic pressure field in the device and hence understand the resultant acoustic radiation force distributions. Both simulated and experimental results are used to track and characterize the evolution of the acoustic radiation force patterns as a function of the fractional order.

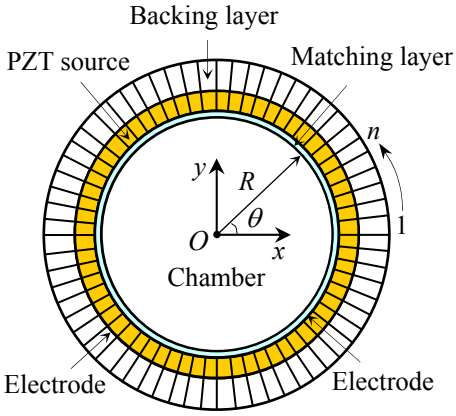

Fig. 1: (Colour on-line) Schematic diagram of the annular array made up of 64 piezoelectric sources as well as matching and backing layers. The vortices are formed in the central chamber which is filled with a water and particle mixture.

Experimental and simulation methods. - Figure 1 shows a schematic diagram of the annular array [24], which consists of 64 individually addressable piezoelectric sources arranged at a pitch of 0.54 mm around a ring with a radius, R = 5.49 mm. The inner surface of the sources is coated with a quarter-wavelength matching layer and the outer surface with a matched absorbing layer which together minimize the reflection of acoustic waves from the boundaries of the internal fluid-filled chamber. The central volume is filled with a mixture of degassed water and microparticles and sealed top and bottom with two thin glass coverslips to produce a cylindrical chamber, which has a height of 2 mm.

In this study, sinusoidal signals with frequency of 2.4 MHz and peak to peak voltage of 25 V are supplied to the individually addressable piezoelectric elements causing them to emit ultrasonic waves. The corresponding wavelength, λ, of the ultrasonic waves in the water is 620 μm. The phase delay for the nth element is given by

$$\phi_n = \frac{2\pi m}{N/G} \cdot \mathrm{mod}(n, N/G)\ , (n = 1, 2, \ldots \ldots, N), \tag{1}$$

where N is the number of active elements, G the number of groups, m the vortex order. The operator mod(,) denotes the operation of modulus after division (or modulo). Note that N = 64 when G = 1, 2, 4 and N = 63 when G = 3. We

observe the central chamber from the *z*-direction with a microscope and use household flour microparticles with diameters ranging from 1 μm to 20 μm [26], a density of 1.47×10^3 kg/m^3 [27] and a sound speed of 2.3×10^3 m/s [28] to visualize the acoustic radiation force field. The microscope, which has a depth of field of 40 μm, is focused midway between the top and bottom coverslips and images are taken before the particles have settled.

A two-dimensional acoustic simulation (in the *x*-*y* plane shown in fig. 1) of the 64-source array is built using finite element analysis (COMSOL Multiphysics, Acoustics module) and used to calculate the acoustic pressure, *p*, and particle velocity, *v*, within the central chamber. The force on spherical particles is given by $\vec{F} = -\nabla U$, where *U* is the Gor'kov potential which can be calculated from the simulated pressure and particle velocity as [29],

$$U = 2\pi a^3 \left[\left(\overline{p^2} / 3\rho c^2 \right) f_1 - (\rho \overline{v^2} / 2) f_2 \right], \tag{2}$$

where *a* is the radius of the spherical particle, $\overline{p^2}$ and $\overline{v^2}$ are the mean-square fluctuations of the pressure and velocity of the acoustic field at the point where the particle is located and ρ and *c* are the density and sound speed of host medium, respectively. The acoustophoretic contrast factors f_1 and f_2 are given by $f_1 = 1 - \rho c^2 / \rho_s c_s^2$ and $f_2 = 2(\rho_s - \rho)/(2\rho_s + \rho)$, where ρ_s and c_s are the density and sound speed of the particle. Here, $\rho = 1\times10^3$ kg/m^3 and $c = 1.48\times10^3$ m/s are used for water. Small dense spheres are expected to move to local minima of the normalized Gor'kov potential, $U/2\pi a^3$.

Results and discussion. - In the first experimental case, all 64 sources are operated as a single group, *i.e.*, $G = 1$. The phase delay from the first source to the last source linearly increases to $2m\pi$ with a phase increment of $2m\pi/64$ between neighboring elements as per eq. (1). In fig. 2 the previously observed family of Bessel-shaped patterns [30,31], are seen for integer orders ($m = 0$, 1 and 2). As expected, the central trap of the first-order Bessel-shaped vortex is small, which is ideal for manipulating single microparticles [24]. The central trap of the second-order Bessel vortex is larger than that of the first-order and its center is no longer a Gor'kov potential minimum. Experimentally we observe two distinct clusters within this central region, which we believe is due to small source

output differences breaking the expected axis-symmetry.

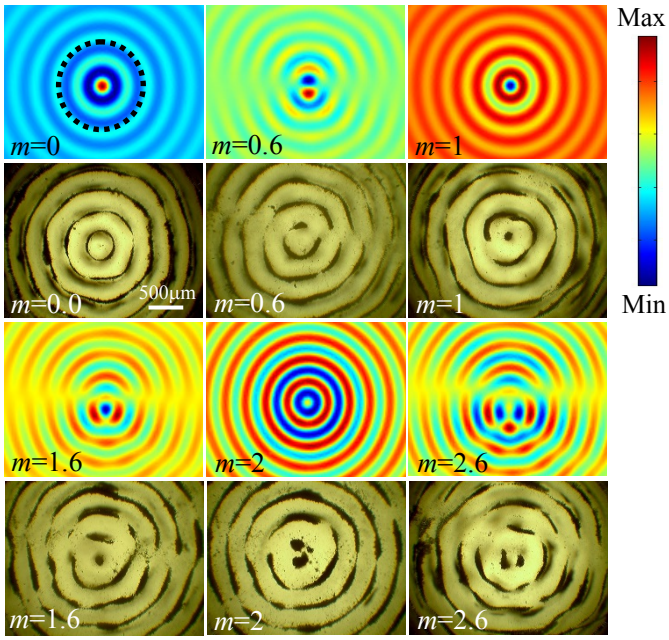

Fig. 2: (Colour on-line) Simulated normalized Gor'kov potential and experimental patterns of integer and fractional acoustic vortices. Parameters $N = 64$, $G = 1$ and m varying from 0 to 2.6. The region of particular interest lies within a radius of λ and is marked by the black doted circle in the top-left plot.

Figure 2 also shows the non-integer orders $m = 0.6$, 1.6 and 2.6, and these exhibit clear asymmetry. In particular, strips oriented in the x-direction, can be observed along which the trapping circles are discontinuous. This phenomena is analogous to the low-intensity radial gaps seen in the cross-sections of fractional optical vortices [13,15,16,19] and is caused by the presence of localized phase discontinuities. In addition to this force discontinuity we also observe a subtle evolution of the shape of the trap center: a short dash when $m = 0.6$, a dash and point when $m = 1.6$ and dash and two points when $m = 2.6$. These trap patterns can be further tuned by varying m between the values seen in this figure.

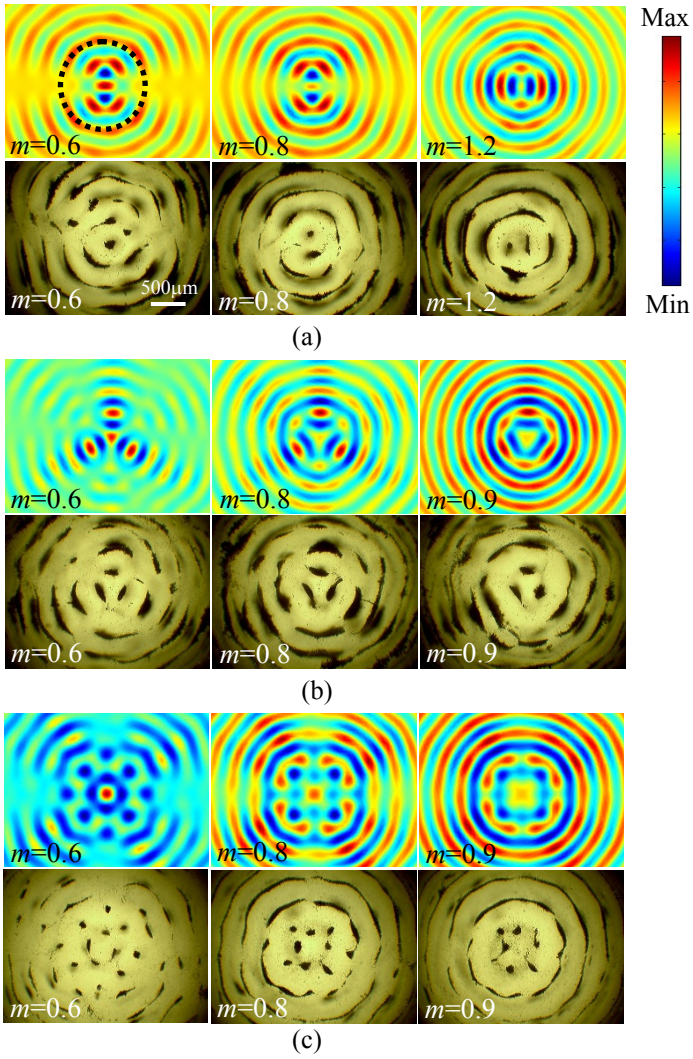

Fig. 3: (Colour on-line) Simulated normalized Gor'kov potential and experimental observations of trapped flour microparticles. (a) $N = 64$, $G = 2$ and m from 0.4 to 1.2; (b) $N = 63$, $G = 3$ and m from 0.6 to 0.9; (c) $N = 64$, $G = 4$ and m from 0.6 to 0.9.

To create $G = 2$, the 64 sources are divided into 2 groups, where the first group includes sources 1-32 and the second group includes the remaining sources. In each group, a linear phase ramp is applied up to $2m\pi$ according to eq. (1) and the order m allowed to change fractionally. As shown in fig. 3(a), the trap patterns of these new acoustic vortices have mirror symmetry about the x- and y-axis. As in the $G = 1$ case, low intensity radial strips near the x-axis appear when $m = 0.6$ and 0.8, which follow a phase discontinuity. It can also be seen that two central deep traps of

small size occur either side of the x-axis when $0.4 < m < 1$ and either side of the y-axis when $1 < m < 1.5$. The distance between these two traps is less than one wavelength and can be tuned by changing m. We later show that this effect can be used to manipulate two particles (or distinct clusters) separated by less than one wavelength. Our observations show that in an $m = 0.6$ vortex, the two trapped clusters of flour microparticles spin rapidly in the same direction (See Supplementary Video [32]), suggesting that orbital angular momentum accompanies these fractional acoustic vortices [33-35].

G= 3 is explored by dividing 63 sources into 3 groups (the 64th element is turned off). As previously, each group is excited using a linear phase ramp according to eq. (1). As shown in fig. 3(b), the trap patterns for $G = 3$ vortices have a rotational symmetry of order 3. A triangular central trapping pattern is found when $0.5 < m < 1$ and the size of the triangle can be tuned by changing m. Figure 3(c) shows that when all 64 sources are divided into 4 groups, *i.e.*, $G = 4$, the resulting vortices have a rotational symmetry of order 4. It is now apparent that the symmetry order corresponds to G. Central traps with a matrix of points are observed when $0.5 < m < 1$. When $m = 0.6$, there are 12 distinguishable points and when $m = 0.8$, there are 8 distinguishable points. With the increase of m from 0.6 towards unity, these points start to merge and form a compact square pattern.

Controlled approach of two microparticles. - As a demonstration of the possible application of fractional order vortices, we use the $G = 2$ patterns shown in fig. 3(a) to manipulate two 90-μm-diameter polystyrene microparticles (Bang Laboratories ltd) with a density of 1.062×10^3 kg/m^3 and a sound speed of 2.4×10^3 m/s. Figure 4(a) shows the two microparticles trapped in the two central Gor'kov potential minima when the vortex order is increased from $m =$ 0.4 towards unity. As the order increases so the distance between the two microparticles varies from 430 μm (0.7λ) to180 μm (0.3λ). Also shown in Fig 4(a) is the simulated phase distribution, from which it can be seen that the particles are trapped at two screw phase singularities which approach as m increases from 0.4 towards unity. In essence the fractional order vortex has created multiple local vortices. Figure 4(b) shows that minima in the

simulated Gor'kov potential are co-located with the phase singularities and the gradient around these minima reduces with increasing m, making the traps less stiff (*i.e.* the traps become less effective). Figure 4(c) shows a comparison between the location of the Gor'kov potential minima from the simulation and the observed location of the polystyrene microparticles. The agreement between simulation and experiment is generally good and it can be seen that the closest approach of the particles is 180 μm (equal to 0.3λ or 2×particle diameter). The small difference between the simulation and experimental curves could be because no secondary scattering was considered in the model. This achieved closest approach is a significant improvement on that possible with one- and two-dimensional orthogonal standing waves ($\lambda/2$) [36,37] and the method of superposition of two first-order Bessel-shaped acoustic vortices (theoretically $L > 0.6\lambda$ and experimentally $L \geq 0.7\lambda$) [24].

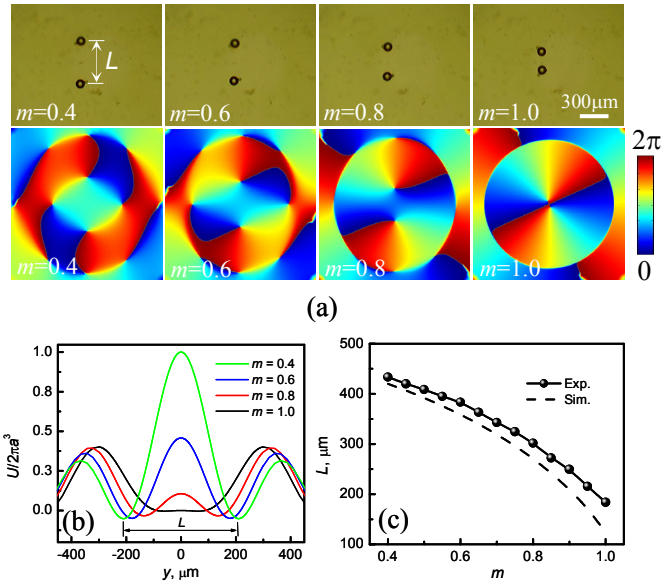

Fig. 4: (Colour on-line) Manipulation of two single 90-μm-diameter polystyrene microparticles using the control parameters N = 64, G = 2 and m from 0.4 to 1.0. (a) Experimental images (top row) and simulated phase (bottom row); (b) simulated normalized Gor'kov potential for x = 0; (c) experimental and simulated m-L curves.

Conclusions. - In summary, two-dimensional fractional acoustic vortices have been generated using a 64-source

annular array. The shapes of the central traps can be controlled by grouping the sources and exciting each group with a suitably chosen phase ramp. The resultant acoustic vortices show a fascinating variety of shapes: points, dashes, triangles and squares. Once a particular pattern is chosen, its size can be tuned by changing the vortex order. For example, if the vortex order is swept from 0.1 towards unity for $G = 2$, it was shown possible to manipulate objects to within 0.3λ. Together these related families of acoustic vortices open up a number of opportunities for the controlled manipulation and rotation of microscale matter.

* * *

This work was supported by China Scholarship Council, National Natural Science Foundation of China (Grant No. 51327901), Fundamental Research Funds for the Central Universities (Grant No. 3102015ZY080) and Pump Priming Grant from University of Bristol. We are grateful to B. Wei for his consistent support.

REFERENCES

[1] Nye J. F. and Berry M. V., *Proc. R. Soc. A*, **336** (1974) 165.

[2] Heckenberg N. R., McDuff R. G., Smith C. P., Rubinsztein-Dunlop H. and Wegerner M. J., *Opt. Quant. Electron.*, **24** (1992) S951.

[3] Mair A., Vaziri A., Weihs G. and Zeilinger A., *Nature*, **412** (2001) 313.

[4] He H., Friese M. E. J., Heckenberg N. R. and Rubinsztein-Dunlop H., *Phys. Rev. Lett.*, **75** (1995) 826.

[5] Franke-Arnold S., Allen L. and Padgett M., *Laser Photon. Rev.*, **2** (2008) 299.

[6] Dienerowitz M. and Dholakia K., *Topologica*, **2** (2009) 008.

[7] Volke-Sepulveda K., Santillan A. O. and Boullosa R. R., *Phys. Rev. Lett.*, **100** (2008) 024302.

[8] Demore C. E. M., Yang Z. Y., Volovick A., Cochran S., MacDonald M. P. and Spalding G. C., *Phys. Rev. Lett.*, **108** (2012)194301.

[9] Anhauser A., Wunenburger R. and Brasselet E., *Phys. Rev. Lett.*, **109** (2012) 034301.

[10] Cai X., Wang J., Strain M. J., Johnson-Morris B., Zhu J., Sorel M., O'Brien J. L., Thompson M. G. and Yu S., *Science*, **338** (2012) 363.

[11] Bozinovic N., Yang Y., Ren Y., Tur M., Kristensen P., Huang H., Willner A. E. and Ramachandran S., *Science*, **340** (2013) 1545.

[12] Beijersbergen M. W., Coerwinkel R. P. C., Kristensen M. and Woerdman J. P., *Opt. Commun.*, **112** (1994) 321.

[13] Tao S. H., Lee W. M. and Yuan X.-C., *Opt. Lett.*, **28** (2003)1867.

[14] Berry M. V., *J. Opt. A*, **6** (2004) 259.

[15] Leach J., Yao E. and Padgett M. J., *New J. Phys.*, **6** (2004) 71.

[16] Lee W. M., Yuan X.-C. and Dholakia K., *Opt. Commun.*, **239** (2004) 129.

[17] Tao S. H., Yuan X.-C., Lin J., Peng X. and Niu H. B., *Opt. Express*, **13** (2005) 7726.

[18] Gotte J. B., O'Holleran K., Preece D., Flossmann F., Franke-Arnold S., Barnett S. M. and Padgett M. J., *Opt. Express*, **16** (2008) 993.

[19] Vyas S., Singh R. K. and Senthilkumaran P., *Opt. Laser Technology*, **42** (2010) 878.

[20] Guo C. S., Yu Y. N. and Hong Z. P., *Opt. Commun.*, **283** (2010) 1889.

[21] Fang G. J., Sun S. H. and Xiong J. X., *Acta Phys. Sin.*, **61** (2012) 064210.

[22] Kang S. T. and Yeh C. K., *IEEE Transactions on Ultrasonics, Ferroelectrics, and Frequency Control*, **57** (2010) 1451.

[23] Mitri F. G., *IEEE Transactions on Ultrasonics, Ferroelectrics, and Frequency Control*, **58** (2011) 662.

[24] Courtney C. R. P., Demore C. E. M., Wu H. X., Grinenko A., Wilcox P. D., Cochran S. and Drinkwater B. W., *Appl. Phys. Lett.*, **104** (2014) 154103.

[25] Dennis M. R., King R. P., Jack B., O'Holleran K. and Padgett M. J., *Nature Physics*, **6** (2010) 118.

[26] Hareland G. A., *J. Cereal Sci.*, **21** (1994) 183.

[27] Ibarz A. and Barbosa-Canovas G. V., *Introduction to Food Process Engineering* (CRC Press, Boca Raton) 2014, p. 263.

[28] Braunstein D., Page J. H., Strybulevych A., Peressini D. and Scanlon M. G., *IOP Conf. Series: Materials Science and Engineering*, **42** (2012) 012040.

[29] Gor'kov L. P., *Sov. Phys. Dokl.*, **6** (1962) 773.

[30] Grinenko A., Wilcox P. D., Courtney C. R. P. and Drinkwater B. W., *Proc. R. Soc. A*, **468** (2012) 3571.

[31] Grinenko A., MacDonald M. P., Courtney C. R. P., Wilcox P. D., Demore C. E. M., Cochran S. and Drinkwater B. W., *Opt. Express*, **23** (2015) 26.

[32] See supplementary video at

[33] Zhang L. and Marston P. L., *J. Acoust. Soc. Am.*, **136** (2014) 2917.

[34] Schwarz T., Petit-Pierre G. and Dual J., *J. Acoust. Soc. Am.*, **133** (2013) 1260.

[35] Foresti D. and Poulikakos D., *Phys. Rev. Lett.*, **112** (2014) 024301.

[36] Wood C. D., Cunningham J. E., O'Rorke R. D., Wälti C., Linfield E. H., Davies A. G. and Evans S. D., *Appl. Phys. Lett.*, **94** (2009) 054101.

[37] Meng L., Cai F., Chen J., Niu L., Li Y., Wu J. and Zheng H., *Appl. Phys. Lett.*, **100** (2012) 173701.